Improved Thermoelectric Properties in Melt-Spun SnTe

Dorra Ibrahim, Viktoriia Ohorodniichuk, Christophe Candolfi, Christopher Semprimoschnig, Anne Dauscher, Bertrand Lenoir

ACS OMEGA

Article

Cite This: ACS Omega 2017, 2, 7106-7111

http://pubs.acs.org/journal/acsodf

Improved Thermoelectric Properties in Melt-Spun SnTe

Dorra Ibrahim,[†] Viktoriia Ohorodniichuk,[†] Christophe Candolfi,*[,†] Christopher Semprimoschnig,[‡] Anne Dauscher,[†] and Bertrand Lenoir[†]

[†]Institut Jean Lamour, UMR 7198 CNRS—Université de Lorraine, 2 allée André Guinier—Campus ARTEM, BP 50840, 54011 Nancy Cedex, France

[‡]European Space Agency, ESTEC, P.O. Box 299, Keperlaan 1, 2200 AG Noordwijk, The Netherlands

Supporting Information

ABSTRACT: SnTe has been the focus of numerous experimental and theoretical studies over the last years owing to its high thermoelectric performances near 800 K when appropriately doped. Here, we demonstrate that melt-spinning, an ultrafast-quenching synthesis technique, followed by spark plasma sintering results in enhanced *ZT* values in polycrystalline SnTe. To illustrate the impact of this technique, the results are contrasted with those obtained on two polycrystalline samples prepared by direct quenching of molten SnTe and without quenching. SnTe melt-spun ribbons are characterized by a peculiar columnar microstructure that contributes to lower the lattice thermal conductivity below 700 K in pressed samples. More importantly, this technique results in a significant decrease in the hole concentration, giving rise to enhanced thermopower values above 500 K. The variation in the hole concentration is likely due to a slight loss of elemental Te during the melt-spinning process. Thanks to the decreased hole concentration, the thermoelectric performances are significantly enhanced with a peak *ZT* value of 0.6 at 800 K, which represents a 40% increase over the values measured for samples prepared with and without quenching. These findings indicate that melt-spinning provides a novel strategy to improve the thermoelectric properties of SnTe that could be worthwhile extending to substituted compounds.

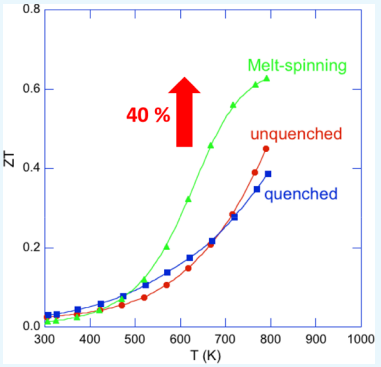

INTRODUCTION

Thermoelectric modules provide the remarkable possibility to directly convert heat into electricity (thermoelectric generators) or vice versa (Peltier coolers).[1−3] Despite its success in space applications, this technology still remains in its infancy owing to the low efficiency achieved in current thermoelectric modules.[1−3] The dimensionless thermoelectric figure of merit $ZT = \alpha^2 T/\rho(\kappa_L + \kappa_e)$ is the key material parameter that governs the efficiency of energy conversion.[1] A good thermoelectric material must meet a subtle balance between a large thermopower (α), a low electrical resistivity (ρ), and low lattice (κ_L) and electronic (κ_e) thermal conductivities. Except for κ_L which is tied to phonon transport, all the transport coefficients are interdependent on each other through the carrier concentration. The best compromise between thermal and electrical transport is usually achieved in heavily doped semiconductors crystallizing into complex crystal structures.[1−3]

Over the last few years, the thermoelectric properties of the simple binary SnTe have been revisited, demonstrating that good thermoelectric performances could be achieved at high temperatures.[4−22] This lead-free analogue of the conventional thermoelectric material PbTe crystallizes in the rock salt structure composed of a face-centered cubic lattice of Te atoms with Sn filling all of the octahedral voids.[23] In addition to being a topological crystalline insulator,[24] the electronic band structure of SnTe mirrors that of PbTe with the presence of a direct band gap at the *L* point in the Brillouin zone (~0.18 eV) and two nondegenerate valence bands at the *L* and Σ points.[25−28] These two bands give rise to simultaneous contributions of heavy and light holes to the transport. The only difference between SnTe and PbTe is related to the energy separation between these two bands which is significantly higher in SnTe (~0.3−0.4 eV) compared to that in PbTe (~0.1 eV).[26−28] Furthermore, SnTe is systematically off-stoichiometric because of a large concentration of Sn vacancies which act as double acceptors resulting in a p-type carrier concentration on the order of 10^{21} cm^{-3} at 300 K.[29,30] Hence, the chemical formula of this compound should be rigorously written as $Sn_{1-z}Te$ with $0.004 \leq z \leq 0.043$ at 873 K (hereafter, we nevertheless keep the formula SnTe to follow the convention used in the literature).[28,29,31] Such large hole concentration leads to metallic properties that can be tuned by either substitution in the Sn or Te sites or introduction of an Sn excess, both of which compensate the Sn vacancies.[4−22] The chemical flexibility of SnTe, which can accommodate a large number of substituting elements,[4−22] offers a plethora of possibilities to optimize its thermoelectric properties, leading to *ZT* values ranging between 1.0 and 1.5 near 800−900 K.[4−22] SnTe exhibits lattice thermal conductivity values on the order of ~2.5 W m^{-1} K^{-1} at 300 K,[4−22] which can be further lowered

Received: September 19, 2017
Accepted: October 11, 2017
Published: October 23, 2017

DOI: 10.1021/acsomega.7b01397
ACS Omega 2017, 2, 7106−7111

by the formation of nanoprecipitates in addition to mass fluctuations introduced by substitutions.[15,20,22]

The melt-spinning technique, which consists of ultrafast quenching of molten compounds on a water-cooled rotating wheel, has been employed to produce ribbons, flakes, or foils with unique nanoscale structures that can potentially help to reduce significantly the thermal transport. In particular, this technique has been successfully used to modulate the thermoelectric properties of Bi_2Te_3-based alloys near room temperature or of skutterudites at high temperatures in the past decades.[32−39] Here, we demonstrate that this technique can be equally applied to produce SnTe ribbons with enhanced thermoelectric properties compared to samples synthesized by conventional techniques. Our results show that the hole concentration in SnTe sensitively depends on the synthetic conditions used. The ultrafast cooling rate achieved in melt-spinning (estimated to be as high as 10^4 to 10^7 K s^{-1}) results in lower hole concentrations with respect to conventional synthesis techniques and hence in higher ZT values that reach 0.6 at 800 K. These results demonstrate that melt-spinning is a rapid and efficient technique to produce polycrystalline SnTe with optimized thermoelectric properties.

RESULTS AND DISCUSSION

The powder X-ray diffraction (PXRD) patterns, shown in Figure 1, were collected on ground melt-spun ribbons and unquenched and quenched samples. The three patterns can be fully indexed within the space group $Fm\bar{3}m$ of SnTe, indicating the absence of secondary phases within the detection limits of PXRD. These analyses further show that SnTe ribbons were successfully produced by melt-spinning. The comparison of the three patterns reveals clear differences in the relative intensities of the Bragg reflections between the melt-spun sample and the two other samples with, in particular, a strong renormalization of the intensity of the (200) and (222) reflections, indicating that the melt-spun ribbons are textured.

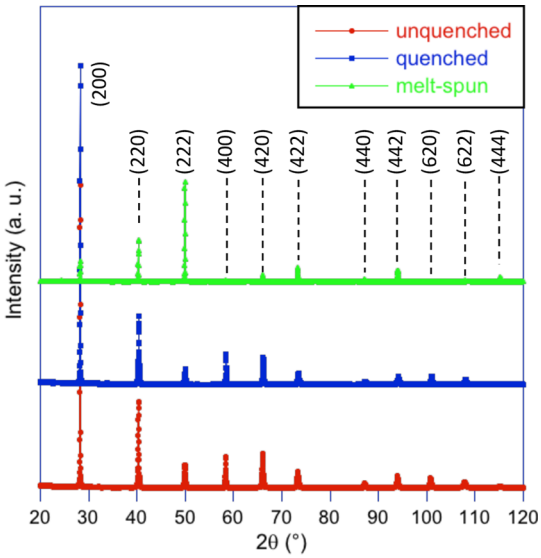

Figure 1. XRD patterns obtained on ground unquenched and quenched ingots and ground melt-spun ribbons. The main reflections are indexed.

The lattice parameters, inferred from Rietveld refinements, are a = 6.3219(3), 6.3119(4), and 6.3240(4) Å for the unquenched, quenched, and melt-spun samples, respectively, which are in good agreement with the literature data.[4−22] A prior study on self-compensated $Sn_{1+x}Te$ ($0 \le x \le 0.04$) has demonstrated a clear correlation between the lattice parameter and the hole concentration, making the former a sensitive measure of the composition in these compounds.[5] The results showed that the lattice expands as Sn vacancies are compensated by Sn excess up to x = 0.03, resulting in a concomitant decrease in the hole concentration.[5] Thus, the higher lattice parameter in the melt-spun sample suggests that the hole concentration is lower in comparison to that in the two other samples. As we will see below, this assumption is confirmed by Hall effect measurements.

To gain relevant insights into the microstructure of the melt-spun ribbons, scanning electron microscopy (SEM) analyses were performed on a randomly selected ribbon on the surface that was in contact with the wheel, on the free surface, and on the cross section (Figure 2). The surface in contact (Figure 1a−c) consists of micron-sized grains in addition to nano-sized particles, whereas a different microstructure is observed on the free surface (Figure 1d−f). These analyses further reveal the presence of a Sn-rich phase in some grains of both surfaces (visible as bright spots in Figure 1a,b,c,e,f), which is systematically observed at the center of the grain (Figure 1a−c). The segregation of elemental Sn is in agreement with the inherent off-stoichiometry of SnTe owing to Sn vacancies. While Sn and Te are homogeneously distributed in all of the pressed samples as indicated by energy-dispersive X-ray spectroscopy (EDXS) analyses (Figures S1−S3 in the Supporting Information), some weak but discernible inhomogeneities are present on the ribbon's surface that was in contact with the wheel (Figure 3) because of the high quenching rate achieved. This inhomogeneous distribution is not visible on the free surface of the ribbons (Figure 3).

The temperature dependences of the measured electrical resistivity and thermopower on the three samples are shown in Figure 4a,b, respectively. Regardless of the synthesis technique used, ρ shows a metallic temperature dependence in the whole temperature range in agreement with the intrinsic metallic nature of SnTe.[4−22] The technique used has virtually no influence on the ρ values which remain nearly constant to ∼1.8 $\mu\Omega$ m at 300 K. At higher temperatures, however, the ρ values of the melt-spun sample increase substantially more with temperature than those of the two other samples. The temperature dependences of α (Figure 3b) are consistent with the ρ data with the highest values observed in the melt-spun sample above 500 K. Below this temperature, the α values are lower in the melt-spun sample than those in the two other samples which exhibit similar values. Above 650 K, this trend reverses, and the melt-spun sample shows the highest values at 800 K. Both this trend reversal and the faster rise in α observed in the melt-spun sample have been attributed to the subtle balance between the contributions of the heavy- and light-hole bands with the former manifesting itself at high temperatures.[4−22] The temperature dependences of ρ and α are typical to those widely observed in pristine and doped SnTe compounds where both properties increase with increasing either the concentration of the substituting element or the Sn excess in self-compensated samples $Sn_{1+x}Te$.[4−22] The trend observed in the electrical properties is thus consistent with the assumption that melt-spinning leads to a decrease in the hole concentration with respect to conventional techniques.

DOI: 10.1021/acsomega.7b01397
ACS Omega 2017, 2, 7106−7111

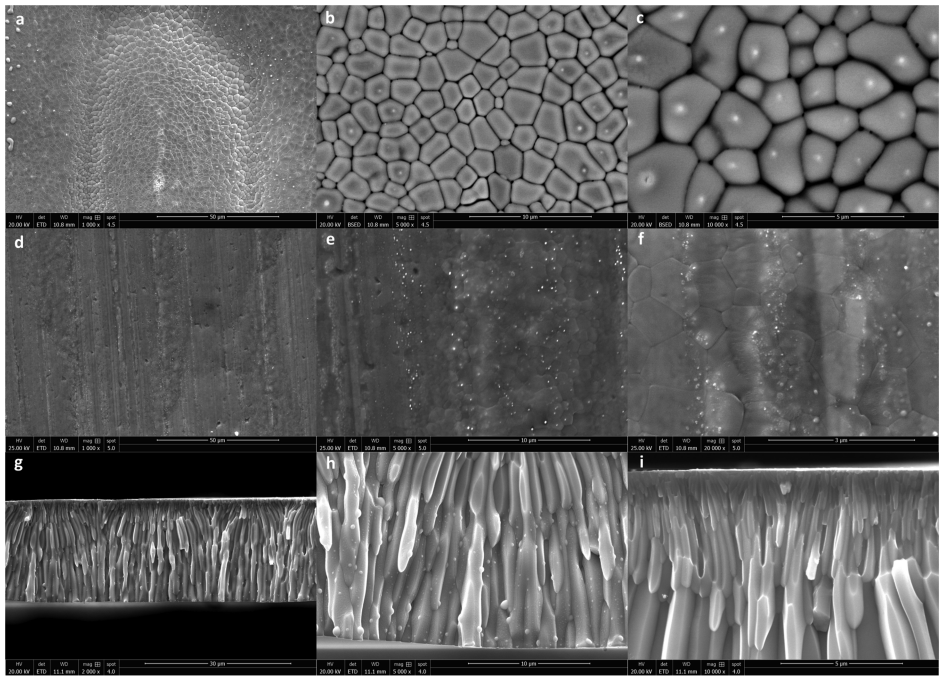

Figure 2. SEM images at different magnifications of a top view of the contact surface (a–c), of the free surface (d–f), and of a cross section (g–i) of SnTe ribbons, revealing the columnar microstructure induced by melt-spinning.

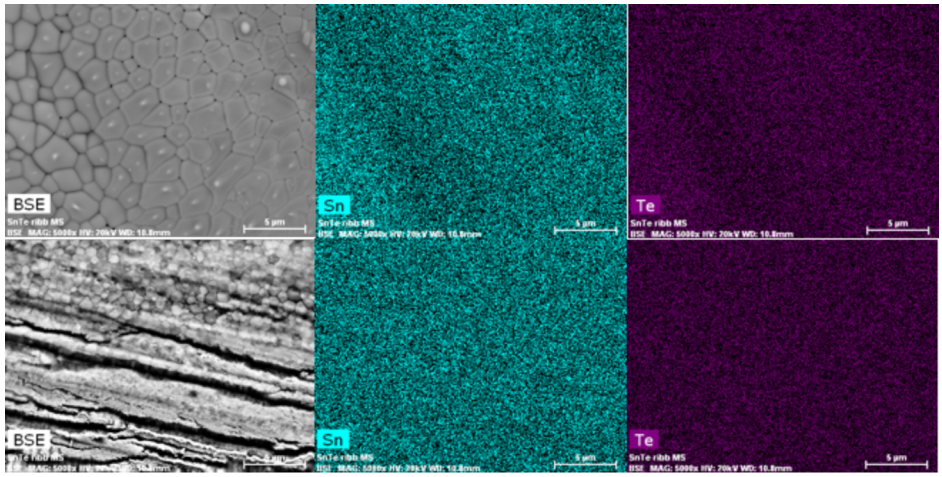

Figure 3. Backscattered electron images and corresponding elemental X-ray maps of the contact surface (upper row) and of the free surface (lower row) of melt-spun SnTe ribbons.

Hall measurements' data measured at 300 K confirm this scenario with R_H values which are significantly lower in the unquenched and melt-spun samples than that in the quenched sample. Within a single-carrier picture, these values yield estimates of the hole concentration p of 1.2×10^{20}, 2.9×10^{20}, and 1.1×10^{21} cm^{-3} in the melt-spun, unquenched, and quenched samples, respectively. The hole concentration in the melt-spun sample is equivalent to that obtained in self-compensated compounds where hole concentrations on the order of 10^{20} cm^{-3} have been achieved.[5] The influence of melt-spinning on the hole concentration is possibly due to slight sublimation of Te that occurs before the molten compound is ejected through the nozzle. This loss of Te partially compensates Sn vacancies, thereby decreasing the hole concentration in the ribbons and eventually in the pressed melt-spun sample. Another possibility is related to modifications of the Sn–Te phase diagram because of the strong out-of-equilibrium conditions imposed by this ultrafast quenching as evidenced in the Bi_2Te_3–Sb_2Te_3 solid solution.[40,41] The Hall mobility, μ_H, increases as p decreases with values of 50, 150, and 580 cm^2 V^{-1} s^{-1} for the quenched, unquenched, and melt-spun samples, respectively, which are in good agreement with prior studies.[4−22]

The total thermal conductivity κ, shown in Figure 4c as a function of the temperature, is significantly lowered by melt-spinning in the whole temperature range, whereas the difference between the quenched and unquenched samples is less pronounced. To gain further insights into the influence of the melt-spinning process on κ_L requires an accurate determination of the electronic component κ_e (see Figure 4c). In the case of SnTe, the estimation of κ_e via the Wiedemann–Franz relation $\kappa_e = LT/\rho$, where L is the Lorenz number, is particularly difficult because L critically depends on the hole scattering mechanisms and details of the electronic

DOI: 10.1021/acsomega.7b01397
ACS Omega 2017, 2, 7106–7111

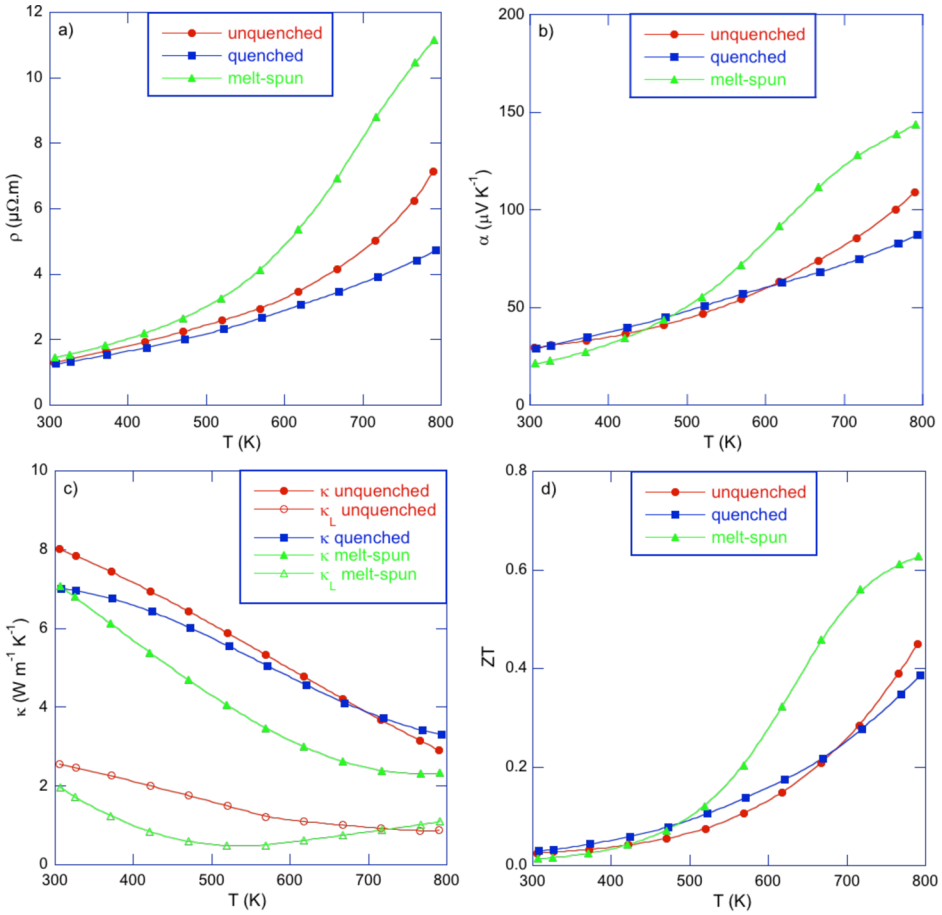

Figure 4. Temperature dependences of the (a) electrical resistivity ρ and (b) thermopower α of the unquenched, quenched, and melt-spun samples. (c) Total (filled symbols) and lattice (open symbols) thermal conductivities as a function of temperature for the three samples. (d) Temperature dependence of the dimensionless figure of merit ZT for the unquenched, quenched, and melt-spun samples. In all panels, the solid lines are guides to the eye.

band structure. In self-compensated and substituted SnTe, the electronic properties have been modeled by considering both parabolic and nonparabolic bands to describe the heavy- and light-hole bands, respectively, with acoustic phonon scattering as the dominant scattering mechanism.[4−22] Both the temperature dependence and L values were found to be highly sensitive to the hole concentration of the sample. However, we found that this two-band model yields overestimated L values, resulting in unphysical κ_L values above 600 K, that is, in the temperature region where the two-band behavior is more pronounced. To overcome this issue, we considered a single-parabolic band model that was used in a prior study to estimate κ_e in the series $Sn_{1+x}Te$.[5] This model, however, breaks down for samples with a hole concentration on the order of 10^{21} cm^{-3} and also leads to unphysical κ_L values. The reason behind this failure is probably related to the multiband electronic structure that governs the transport at high hole concentrations and to a significant change in the density of states effective mass of the nonparabolic band, which is not taken into account in both models. For these reasons, none of these models could be applied to the quenched sample. As shown in Figure 4c, the κ_L values of the melt-spun sample are lower than those derived for the unquenched sample with a minimum value of 0.5 W m^{-1} K^{-1} already reached at 500 K. The increase observed above this temperature for the melt-spun sample is likely an artifact of the single-band model used which does not account for the significant contribution of the heavy-hole band between 600 and 800 K. Keeping in mind the above-mentioned inherent difficulties in estimating κ_e, these results nevertheless seem to indicate that the particular microstructure induced by melt-spinning contributes to limit the phonon transport in SnTe below 700 K in a way similar to that observed in samples containing nanodomains.[14,15,20,22] At higher temperatures, however, the influence of this technique is less pronounced because the lattice thermal conductivity values measured in the melt-spun sample seem to be higher than those achieved in the unquenched sample.

The combination of the three transport properties results in ZT values that increase with increasing temperature (Figure 4d). Because of a decreased hole concentration and steep rise in the thermopower values, the ZT values of the melt-spun sample rapidly increase above 500 K to reach a maximum value of 0.6 at 800 K. The peak ZT value obtained in the melt-spun sample is 40% higher than the maximum values obtained in the unquenched and quenched samples for which a peak ZT value of 0.45 at 800 K is achieved in the former. The results obtained on the melt-spun sample are consistent with prior studies on self-compensated $Sn_{1+x}Te$ compounds where a maximum ZT value of 0.6 has been reported for x = 0.04.[5] However, the lower thermal conductivity values achieved above 500 K in the melt-spun sample contribute to reach higher ZT values between 600 and 800 K than that in the $Sn_{1+x}Te$ samples as a result of a

DOI: 10.1021/acsomega.7b01397
ACS Omega 2017, 2, 7106−7111

shift of the $ZT(T)$ curve toward lower temperatures. Our results thus demonstrate that melt-spinning is an interesting approach to tune the carrier concentration in polycrystalline SnTe to a level equivalent to that obtained in optimized samples. Although the peak ZT value achieved in the melt-spun sample is not enhanced compared to that in optimized samples prepared by conventional synthetic routes,[5] this technique may open a new avenue for optimizing the thermoelectric properties of SnTe-based compounds, which warrants further investigations.

EXPERIMENTAL METHODS

In this study, three polycrystalline samples of SnTe were synthesized by the direct reaction of stoichiometric amounts of Sn shots (99.999%) and Te powders (99.999%) in an equimolar ratio in evacuated and sealed quartz tubes. The ampules were sealed under inert atmosphere, heated to 1133 K over 10 h in a rocking furnace, and maintained at this temperature for 5 h. The first sample was quenched in room-temperature water, whereas the two other samples were furnace-cooled to room temperature. As a second step, one furnace-cooled ingot was used for melt-spinning. The melt-spinning process was performed with a melt-spinner (Bühler) equipped with a copper wheel of ∼20 cm in diameter. The ∼10 g ingot was placed in a quartz tube with a V-shaped end and a nozzle diameter of 1 mm. No additional elemental Te has been added to compensate a possible loss of Te during the heating process. The sample was heated to ∼1133 K under argon atmosphere (0.8 bar) with the temperature continuously monitored by a digital infrared pyrometer (Maurer). The molten sample was ejected from the tube on the copper wheel rotating at 12 m s^{-1} (linear speed) using an overpressure of 1.3 bar of argon. Upon contact with the wheel, the melt was instantaneously cooled, yielding ribbons with dimensions on the order of 7−10 mm in length, 2−3 mm in width, and ∼20 μm in thickness. All of the three samples (quenched, unquenched, and melt-spun) were ground into fine powders and loaded in a 10 mm diameter graphite die. The powders were then consolidated by spark plasma sintering at 773 K for 10 min under a uniaxial pressure of 64 MPa. For all samples, the relative density was above 97% of the theoretical density from XRD data. The nature and phase purity of the samples were verified by PXRD using a Bruker D8 ADVANCE instrument with Cu Kα1 radiation. The chemical homogeneity of the consolidated samples and the microstructure of the ribbons were analyzed by SEM and EDXS using a Quanta FEG 650 (FEI).

For transport property measurements, samples with well-defined shape and dimensions (typically 2 × 2 × 8 mm^3 and 10 mm diameter, 1 mm thickness for bar- and disk-shaped samples, respectively) were cut with a diamond-wire saw from the dense ingots. Thermopower and electrical resistivity were simultaneously measured on bar-shaped samples between 300 and 800 K using a ZEM-3 setup (ULVAC-RIKO). Thermal conductivity was determined in the same temperature range following the relation $\kappa = aC_pd$ where a is the thermal diffusivity, C_p is the specific heat, and d is the experimental density. Thermal diffusivity was measured on disk-shaped samples by the laser flash technique using a Netzsch LFA 427 instrument. The specific heat was measured by differential scanning calorimetry using a Pegasus 403 instrument (Netzsch), while the density was considered temperature-independent. The Hall coefficient R_H was measured at 300 K using the ac transport option of a physical property measurement system (PPMS, Quantum Design). The Hall carrier concentration p and the Hall mobility μ_H of the charge carriers were calculated from the Hall coefficient R_H, assuming a single-carrier picture and a Hall factor r_H of 1 according to the relations $p = r_H/R_He = 1/R_He$ and $\mu_H = R_H/\rho$, where e is the elementary charge.

ASSOCIATED CONTENT

Supporting Information

The Supporting Information is available free of charge on the ACS Publications website at DOI: 10.1021/acsomega.7b01397.

Backscattered electron images and elemental X-ray mappings of the unquenched, quenched, and pressed melt-spun samples (PDF)

AUTHOR INFORMATION

Corresponding Author

*E-mail: christophe.candolfi@univ-lorraine.fr (C.C.).

ORCID

Christophe Candolfi: 0000-0002-1248-5354

Notes

The authors declare no competing financial interest.

ACKNOWLEDGMENTS

The authors thank the financial support from the European Space Agency under NPI contract no. 40001134346/15/NL/RA and from the Région Lorraine.

REFERENCES

(1) Goldsmid, H. J. *Thermoelectric Refrigeration*; Temple Press Books Ltd.: London, 1964.

(2) *Thermoelectrics and Its Energy Harvesting*; Rowe, D. M., Ed.; CRC Press, 2012.

(3) Tan, G.; Zhao, L.-D.; Kanatzidis, M. G. Rationally Designing High-Performance Bulk Thermoelectric Materials. *Chem. Rev.* **2016**, *116*, 12123−12149.

(4) Tan, G.; Shi, F.; Doak, J. W.; Sun, H.; Zhao, L.-D.; Wang, P.; Uher, C.; Wolverton, C.; Dravid, V. P.; Kanatzidis, M. G. Extraordinary role of Hg in enhancing the thermoelectric performance of p-type SnTe. *Energy Environ. Sci.* **2015**, *8*, 267−277.

(5) Tan, G.; Zhao, L.-D.; Shi, F.; Doak, J. W.; Lo, S.-H.; Sun, H.; Wolverton, C.; Dravid, V. P.; Uher, C.; Kanatzidis, M. G. High Thermoelectric Performance of p-Type SnTe via a Synergistic Band Engineering and Nanostructuring Approach. *J. Am. Chem. Soc.* **2014**, *136*, 7006−7017.

(6) Zhang, Q.; Liao, B.; Lan, Y.; Lukas, K.; Liu, W.; Esfarjani, K.; Opeil, C.; Broido, D.; Chen, G.; Ren, Z. High thermoelectric performance by resonant dopant indium in nanostructured SnTe. *Proc. Natl. Acad. Sci. U.S.A.* **2013**, *110*, 13261−13266.

(7) Zhou, M.; Gibbs, Z. M.; Wang, H.; Han, Y.; Xin, C.; Li, L.; Snyder, G. J. Optimization of thermoelectric efficiency in SnTe: the case for the light band. *Phys. Chem. Chem. Phys.* **2014**, *16*, 20741−20748.

(8) Banik, A.; Shenoy, U. S.; Anand, S.; Waghmare, U. V.; Biswas, K. Mg Alloying in SnTe Facilitates Valence Band Convergence and Optimizes Thermoelectric Properties. *Chem. Mater.* **2015**, *27*, 581−587.

(9) Tan, G.; Shi, F.; Hao, S.; Chi, H.; Bailey, T. P.; Zhao, L.-D.; Uher, C.; Wolverton, C.; Dravid, V. P.; Kanatzidis, M. G. Valence Band Modification and High Thermoelectric Performance in SnTe Heavily Alloyed with MnTe. *J. Am. Chem. Soc.* **2015**, *137*, 11507−11516.

(10) He, J.; Tan, X.; Xu, J.; Liu, G.-Q.; Shao, H.; Fu, Y.; Wang, X.; Liu, Z.; Xu, J.; Jiang, H.; Jiang, J. Valence band engineering and

DOI: 10.1021/acsomega.7b01397
ACS Omega 2017, 2, 7106−7111

thermoelectric performance optimization in SnTe by Mn-alloying via a zone-melting method. *J. Mater. Chem. A* **2015**, *3*, 19974−19979.
(11) Tan, G.; Shi, F.; Hao, S.; Chi, H.; Zhao, L.-D.; Uher, C.; Wolverton, C.; Dravid, V. P.; Kanatzidis, M. G. Codoping in SnTe: Enhancement of Thermoelectric Performance through Synergy of Resonance Levels and Band Convergence. *J. Am. Chem. Soc.* **2015**, *137*, 5100−5112.
(12) Tan, G.; Zeier, W. G.; Shi, F.; Wang, P.; Snyder, G. J.; Dravid, V. P.; Kanatzidis, M. G. High Thermoelectric Performance SnTe−In_2Te_3 Solid Solutions Enabled by Resonant Levels and Strong Vacancy Phonon Scattering. *Chem. Mater.* **2015**, *27*, 7801−7811.
(13) Al Rahal Al Orabi, R.; Mecholsky, N. A.; Hwang, J.; Kim, W.; Rhyee, J.-S.; Wee, D.; Fornari, M. Band Degeneracy, Low Thermal Conductivity, and High Thermoelectric Figure of Merit in SnTe−CaTe Alloys. *Chem. Mater.* **2016**, *28*, 376−384.
(14) Zhao, L.-D.; Zhang, X.; Wu, H.; Tan, G.; Pei, Y.; Xiao, Y.; Chang, C.; Wu, D.; Chi, H.; Zheng, L.; Gong, S.; Uher, C.; He, J.; Kanatzidis, M. G. Enhanced Thermoelectric Properties in the Counter-Doped SnTe System with Strained Endotaxial SrTe. *J. Am. Chem. Soc.* **2016**, *138*, 2366−2373.
(15) Banik, A.; Vishal, B.; Perumal, S.; Datta, R.; Biswas, K. The origin of low thermal conductivity in $Sn_{1-x}Sb_xTe$: phonon scattering via layered intergrowth nanostructures. *Energy Environ. Sci.* **2016**, *9*, 2011−2019.
(16) Zhang, L.; Wang, J.; Cheng, Z.; Sun, Q.; Li, Z.; Dou, S. Lead-free SnTe-based thermoelectrics: enhancement of thermoelectric performance by doping with Gd/Ag. *J. Mater. Chem. A* **2016**, *4*, 7936−7942.
(17) Zhou, Z.; Yang, J.; Jiang, Q.; Luo, Y.; Zhang, D.; Ren, Y.; He, X.; Xin, J. Multiple effects of Bi doping in enhancing the thermoelectric properties of SnTe. *J. Mater. Chem. A* **2016**, *4*, 13171−13175.
(18) Al Rahal Al Orabi, R.; Hwang, J.; Lin, C.-C.; Gautier, R.; Fontaine, B.; Kim, W.; Rhyee, J.-S.; Wee, D.; Fornari, M. Ultralow Lattice Thermal Conductivity and Enhanced Thermoelectric Performance in SnTe:Ga Materials. *Chem. Mater.* **2017**, *29*, 612−620.
(19) Roychowdhury, S.; Shenoy, U. S.; Waghmare, U. V.; Biswas, K. An enhanced Seebeck coefficient and high thermoelectric performance in p-type In and Mg co-doped $Sn_{1-x}Pb_xTe$ via the co-adjuvant effect of the resonance level and heavy hole valence band. *J. Mater. Chem. C* **2017**, *5*, 5737−5748.
(20) Li, W.; Zheng, L.; Ge, B.; Lin, S.; Zhang, X.; Chen, Z.; Chang, Y.; Pei, Y. Promoting SnTe as an eco-friendly solution for p-PbTe thermoelectric via Band Convergence and Interstitial Defects. *Adv. Mater.* **2017**, *29*, 1605887.
(21) Wang, L.; Tan, X.; Liu, G.; Xu, J.; Shao, H.; Yu, B.; Jiang, H.; Yue, S.; Jiang, J. Manipulating Band Convergence and Resonant State in Thermoelectric Material SnTe by Mn−In Codoping. *ACS Energy Lett.* **2017**, *2*, 1203−1207.
(22) Zheng, L.; Li, W.; Lin, S.; Li, J.; Chen, Z.; Pei, Y. Interstitial Defects Improving Thermoelectric SnTe in Addition to Band Convergence. *ACS Energy Lett.* **2017**, *2*, 563−568.
(23) Hashimoto, K.; Hirakawa, K. Electrical Properties of Stannous Telluride SnTe. *J. Phys. Soc. Jpn.* **1956**, *11*, 716−717.
(24) Hsieh, T. H.; Lin, H.; Liu, J.; Duan, W.; Bansi, A.; Fu, L. Topological crystalline insulators in the SnTe material class. *Nat. Commun.* **2012**, *3*, 982.
(25) Tanaka, Y.; Ren, Z.; Sato, T.; Nakayama, K.; Souma, S.; Takahashi, T.; Segawa, K.; Ando, Y. Experimental realization of a topological crystalline insulator in SnTe. *Nat. Phys.* **2012**, *8*, 800−803.
(26) Rogers, L. M. Valence band structure of SnTe. *J. Phys. D: Appl. Phys.* **1968**, *1*, 845−852.
(27) Singh, D. J. Thermopower of SnTe from Boltzmann transport calculations. *Funct. Mater. Lett.* **2010**, *03*, 223−226.
(28) Brebrick, R. F.; Strauss, A. J. Anomalous Thermoelectric Power as Evidence for Two-Valence Bands in SnTe. *Phys. Rev.* **1963**, *131*, 104−110.
(29) Brebrick, R. F. Deviations from stoichiometry and electrical properties in SnTe. *J. Phys. Chem. Solids* **1963**, *24*, 27−36.
(30) Kafalas, J. A.; Brebrick, R. F.; Strauss, A. J. Evidence that SnTe is a semiconductor. *Appl. Phys. Lett.* **1964**, *4*, 93−94.
(31) Chigikov, D. M.; Schastliviy, V. P. *Tellurium and Tellurides*; Nauka: Moscow, 1966.
(32) Xie, W.; Tang, X.; Yan, Y.; Zhang, Q.; Tritt, T. M. High thermoelectric performance BiSbTe alloy with unique low-dimensional structure. *J. Appl. Phys.* **2009**, *105*, 113713.
(33) Xie, W.; Tang, X.; Yan, Y.; Zhang, Q.; Tritt, T. M. Unique nanostructures and enhanced thermoelectric performance of melt-spun BiSbTe alloys. *Appl. Phys. Lett.* **2009**, *94*, 102111.
(34) Xie, W.; He, J.; Kang, H. J.; Tang, X.; Zhu, S.; Laver, M.; Wang, S.; Copley, J. R. D.; Brown, C. M.; Zhang, Q.; Tritt, T. M. Identifying the Specific Nanostructures Responsible for the high Thermoelectric Performance of $(Bi,Sb)_2Te_3$ Nanocomposites. *Nano Lett.* **2010**, *10*, 3283−3289.
(35) Ohorodniichuk, V.; Dauscher, A.; Masschelein, P.; Candolfi, C.; Baranek, P.; Dalicieux, P.; Lenoir, B. Investigation of the Nozzle Diameter as a Control Parameter of the Properties of Melt-Spun $Sb_{2-x}Bi_xTe_3$. *J. Electron. Mater.* **2016**, *45*, 1419−1424.
(36) Ohorodniichuk, V.; Candolfi, C.; Masschelein, P.; Baranek, P.; Dalicieux, P.; Dauscher, A.; Lenoir, B. Influence of Preparation Processing on the Transport Properties of Melt-Spun $Sb_{2-x}Bi_xTe_{3+y}$. *J. Electron. Mater.* **2016**, *45*, 1561−1569.
(37) Ohorodniichuk, V.; Dauscher, A.; Lopes, E. B.; Migot, S.; Candolfi, C.; Lenoir, B. Structural and Electrical Properties Characterization of $Sb_{1.52}Bi_{0.48}Te_{3.0}$ Melt-Spun Ribbons. *Crystals* **2017**, *7*, 172.
(38) Tan, G.; Liu, W.; Wang, S.; Yan, Y.; Li, H.; Tang, X.; Uher, C. Rapid preparation of $CeFe_4Sb_{12}$ skutterudite by melt spinning: Rich nanostructures and high thermoelectric performance. *J. Mater. Chem. A* **2013**, *1*, 12657−12668.
(39) Tan, G.; Zheng, Y.; Tang, X. High thermoelectric performance of nonequilibrium synthesized $CeFe_4Sb_{12}$ composite with multi-scaled nanostructures. *Appl. Phys. Lett.* **2013**, *103*, 183904.
(40) Abrikosov, N. K.; Bankina, V. F.; Kolomoets, L. A.; Dzhaliashvili, N. V. Deviation of the solid solution from stoichiometry in the section Bi_2Te_3−Sb_2Te_3 in the region of $Bi_{0.5}Sb_{1.5}Te_3$ composition. *Izv. Akad. Nauk SSSR, Neorg. Mater.* **1977**, *13*, 827−829.
(41) Manyakin, S. M.; Volkov, M. P. Microstructure of $(Bi_{0.25}Sb_{0.75})_2Te_3$ Profiled Crystals Grown by Directed Crystallization Method. *Proceedings of the Twenty-First International Conference on Thermoelectrics*; IEEE: Long Beach, USA, 2002; pp 21−23.

DOI: 10.1021/acsomega.7b01397
ACS Omega 2017, 2, 7106−7111